



Calibration of Hardening Rules for Cyclic Plasticity

M. Rezaiee-Pajand*, S. Sinaie

Department of Civil Engineering, Ferdowsi University of Mashhad, Iran

PAPER INFO

Paper history:

Received 15 July 2012

Received in revised form 04 October 2012

Accepted 18 October 2012

Keywords:

Cyclic Plasticity
Multi-axial Ratcheting
Parameter Determination
Kinematic Hardening
Calibration Methods

ABSTRACT

In the realm of multi-axial ratcheting, a step by step mathematical approach is developed for the parameter determination of decomposed kinematic hardening rules. For this purpose, key characteristics are mathematically derived for these hardening rules under multi-axial loading. Then, these characteristics are utilized to develop expressions which relate the loading history to the accumulated plastic strain. Unlike the calibration techniques available in the literature, this new method does not include trial and error analyses to fit the simulation results to the experimental data. The proposed method is illustrated through a numerical example. The results not only demonstrate the effectiveness of the approach, but also indicate that simple hardening rules, if calibrated accordingly, can be much more efficient than what has been shown before.

doi: 10.5829/idosi.ije.2013.26.04a.04

NOMENCLATURE

σ	Stress tensor	J_2	Second deviatoric stress invariant
s	Deviatoric stress tensor	R_0	Radius of yield surface
α	Backstress tensor	σ_y	Yield stress
a	Deviatoric backstress tensor	$d\lambda$	Plastic multiplier
$d\epsilon^p$	Plastic strain increment tensor	B, γ	Kinematic hardening parameters
$d\epsilon^p$	Deviatoric plastic strain increment tensor	δ	Multi-axial hardening parameter
dp	Effective plastic strain increment	d	Distance of deviatoric stress path to the origin
$f()$	Yield function	d_a	Distance of deviatoric backstress path to the origin
d_s	Distance between the deviatoric stress and deviatoric backstress paths		

1. INTRODUCTION

The accumulation of plastic strain during loading cycles is referred to as ratcheting. Major experimental effort has been made to gain a better understanding of this phenomenon. Experiments conducted by Moyer and Sinclair [1], Benham [2], Freudenthal and Ronay [3],

Ruiz [4], Yoshida et al. [5], Benallal et al. [6], Hassan et al. [7], Hassan and Kyriakides [8-10], Yoshida [11], Delobelle et al. [12], Corona et al. [13], Portier et al. [14], Bocher et al. [15], Aubin et al. [16], Kang et al. [17] and Hassan et al. [18] demonstrate the ratcheting characteristics in various circumstances.

Experiments can be categorized as uniaxial or biaxial. Uniaxial experiments are either stress or strain controlled while biaxial experiments usually incorporate stress in one direction (axial tension or internal

* Corresponding Author Email: mrpajand@yahoo.com (M. Rezaiee-Pajand)

pressure) and strain in another direction (shear strain or axial strain). The rate at which plastic strain is accumulated can be correlated to the parameters of the loading history. In uniaxial loading the rate of ratcheting will only depend on the peak magnitudes of the mean and amplitude stresses and strains [8]. However, in biaxial loading the situation is more complex, since the loading path also becomes pertinent to the matter. An extensive set of biaxial experiments was conducted by Hassan and Kyriakides [10], where they investigated the effect of different mean and amplitude stresses on the rate of ratcheting. Aubin et al. [16] also carried out biaxial experiments. However, their idea was to keep constant values of equivalent mean and amplitude stresses while altering the loading path. Later on, Hassan et al. [18] pursued the same idea where they discussed the effect of non-proportional loading on biaxial ratcheting.

Parallel to experiments, extensive efforts have also been made in the analytical field to simulate the cyclic response of materials. Prager [19] introduced the linear kinematic hardening rule which could model the Bauschinger effect but failed to predict ratcheting. Afterwards, two main modifications were made to this hardening rule. Besseling [20] and Mroz [21] suggested the concept of a multisurface model where each surface evolved according to a linear hardening rule. This idea was further pursued by Dafalias and Popov [22-24] and Krieg [25] which introduced a two-surface model and later by the bounding surface theory of Dafalias [26]. These hardening rules are referred to as multilinear models, since they all resemble a piece-wise linear stress-strain curve. Although the multilinear models were an improvement to Prager's linear hardening rule, but they still failed to simulate ratcheting, since they produced closed hysteresis curves during cyclic loading.

Adding the so called "recovery term" was the other modification made to Prager's linear hardening rule. This added term is meant to take the fading memory of the plastic strain path into account. Therefore, by producing a nonlinear evolution law, make plastic strain accumulation possible. Armstrong and Frederick [27] were first to use a recovery term in their model. Then, a wide range of kinematic hardening rules have been presented using the idea of a strain hardening and a recovery term in the evolution law. Another major improvement made to nonlinear kinematic hardening rules was introduced by Chaboche and his co-workers [28, 29]. They decomposed the backstress into several components, where each of the components individually evolved according to an AF hardening rule. The concept of decomposing the backstress gave the advantage of reproducing the cyclic stress-strain curve more accurately. Afterwards, many researchers have proposed more complex kinematic hardening rules using the idea of a decomposed backstress and various forms of the recovery term. Chaboche [30] and Ohno and Wang [31]

used a modified version of the original AF equation in their decomposed models. Furthermore, in order to improve the high cycle and multiaxial ratcheting simulation, modifications have been made to the Chaboche and Ohno-Wang models by McDowell [32], Jiang and Sehitoglu [33], Voyiadjis and Basuroychowdhury [34], AbdelKarim and Ohno [35], Bari and Hassan [36], Chen and Jiao [37], Chen et al. [38] and others. A detailed review of various plasticity models used for ratcheting simulation can be found in [39].

An important problem regarding ratcheting simulation is to effectively determine the material parameters of the hardening rule. Bari and Hassan [40] determined a number of the material constants by dividing the uniaxial strain controlled hysteresis curve into segments and using the properties of each segment. However, in order to produce a good fit to the uniaxial hysteresis curve, some of the parameters were eventually determined by trial and error. Koo and Lee [41] also used a similar approach in their work. Chen and Jiao [37] determined some of the material constants by utilizing the properties of the monotonic uniaxial tensile curve, while the other parameters were obtained by a trial and error approach. Hassan et al. [18] evaluated the parameters using four different experiments. However, a trial and error method was eventually used to fit the numerical simulation to the experimental data. The problem of a trial and error solution is that its time consuming. Numerous analyses have to be carried out in order to determine reasonable results. Bearing this in mind, Rezaiee-Pajand and Sinaie [42] managed to develop a complete systematic approach to effectively determine the material constants of Chaboche's hardening rule. Their work did not involve any trial and error. In addition, their work indicated that if the hardening parameters are effectively obtained by direct use of ratcheting data, the hardening rule of Chaboche can be much more effective than what had been demonstrated before.

It has been shown that if the parameters of a model are determined using a specific type of experiment, the model will fail to effectively simulate other experiments. Moreover, many models are basically developed by uniaxial hysteresis loops, while others are based on biaxial behavior. According to Bari and Hassan [36] and Chen et al. [38], no model is yet general enough to simulate both uniaxial and multiaxial ratcheting responses effectively. Despite this argument, Bari and Hassan [36] used the idea of Delobelle et al. [12] to introduce a unique hardening parameter into their model. The significance of this parameter is that its value has no effect on the uniaxial response of the model. Therefore, it can be independently calibrated for multiaxial ratcheting simulation. Ever since, many researchers have introduced this multiaxial ratcheting parameter into their hardening models. For example,

Chen and Jiao [37] used an evolutionary form of this parameter. No mathematical procedure of evaluating this parameter is presented in the literature and current works solely rely on trial and error. In order to overcome the time consuming process of trial and error analyses, an effective approach of obtaining this parameter is developed here. In this paper, the calibration process developed in [42] is followed to obtain this systematic approach

2. EXPERIMENTAL DATA

The biaxial experimental data of [7] and [13] conducted on CS 1026 are used to confirm the validity of the proposed methods in this paper. The loading histories are illustrated in Figure 1, while the loading values for each loading history are given in Tables 1 and 2. It should be mentioned here that the calibration process will be developed according to the second set of loading values for the axial strain cycle with constant internal pressure loading history (test-2), while the bow-tie loading history is used to evaluate the accuracy of the results.

3. DESCRIPTION OF HARDENING PLASTICITY MODELS

The von Mises yield surface can be written as:

$$f(\bar{\mathbf{s}}) = \sqrt{(\mathbf{s} - \mathbf{a})(\mathbf{s} - \mathbf{a})} = \sqrt{\bar{\mathbf{s}} \cdot \bar{\mathbf{s}}} = \sqrt{2\bar{J}_2} = R_0 \quad (1)$$

where \mathbf{s} and \mathbf{a} are the deviatoric stress and backstress tensors, respectively. In addition, $\mathbf{s} - \mathbf{a}$ is denoted by $\bar{\mathbf{s}}$ for mathematical convenience, whereby $2\bar{J}_2 = \bar{\mathbf{s}} \cdot \bar{\mathbf{s}}$. The value of R_0 indicates the radius of the yield surface in the deviatoric plane. Therefore, if only kinematic hardening is implemented, its value will be constant and equal to $R_0 = \sqrt{2/3}\sigma_y$. In addition, the following will also be valid for the gradient of the yield surface:

$$\frac{\partial f}{\partial \bar{\mathbf{s}}} = \frac{\partial f}{\partial \bar{\mathbf{s}}} = \frac{\bar{\mathbf{s}}}{\sqrt{2\bar{J}_2}} = \frac{\bar{\mathbf{s}}}{R_0} \quad (2)$$

Since the value of $2\bar{J}_2$ is constant during plastic flow (equal to R_0^2), the following can be obtained by differentiation:

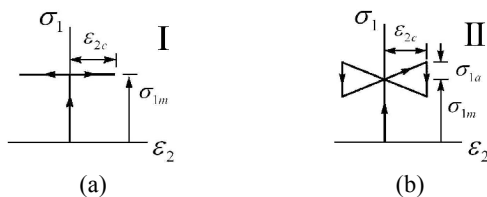


Figure 1. Biaxial loading histories. (a) axial strain cycle with constant internal pressure (b) bow-tie cycle.

TABLE 1. Loading values for the axial strain cycle with constant internal pressure loading history (case I)

Test No.	1	2	3	4	5	6
σ_{1m} (MPa)	66.5	66.5	66.5	33.6	50.5	100.3
ε_{2c} (%)	0.40	0.50	0.65	0.50	0.50	0.50

TABLE 2. Loading values for the bow-tie loading history (case II)

Test No.	7	8
σ_{1m} (MPa)	66.5	100.3
σ_{1a} (MPa)	16.3	16.3
ε_{2c} (%)	0.50	0.50

$$d(2\bar{J}_2) = d(\bar{\mathbf{s}} \cdot \bar{\mathbf{s}}) = \bar{\mathbf{s}} \cdot d\bar{\mathbf{s}} + \bar{\mathbf{s}} \cdot (d\mathbf{s} - d\mathbf{a}) = 0 \quad (3)$$

This result can also be obtained by utilizing the consistency condition, which ensures that the stress state will always remain on the yield surface during plastic flow.

An associated flow rule is assumed for the model, which indicates that the direction of the plastic strain increment is in the direction of the gradient of the yield surface:

$$d\boldsymbol{\varepsilon}^p = d\lambda \frac{\partial f}{\partial \bar{\mathbf{s}}} = d\lambda \frac{\bar{\mathbf{s}}}{R_0} \quad (4)$$

The evolution of the backstress is governed by a kinematic hardening rule. Various forms of the hardening rule exist in the literature [39]. However, only the ones concerning the development of the present work will be presented here. Although these hardening rules are usually described in the general stress and strain spaces, but, since a von Mises yield surface is used, all of the relations can also be rewritten in terms of deviatoric components.

3. 1. The Armstrong-Frederick Nonlinear Kinematic Hardening Rule

Armstrong and Frederick [27] proposed their nonlinear rule in the following form:

$$\begin{aligned} d\mathbf{a} &= \frac{2}{3} B d\boldsymbol{\varepsilon}^p - \gamma \mathbf{a} dp \\ dp &= \sqrt{\frac{2}{3}} d\boldsymbol{\varepsilon}^p d\boldsymbol{\varepsilon}^p = \sqrt{\frac{2}{3}} d\lambda \end{aligned} \quad (6)$$

It can be seen that a combination of $\bar{\mathbf{s}}$ and \mathbf{a} is used to define the direction of the backstress increment.

3. 2. The Burlet-Cailletaud Nonlinear Hardening Rule

Burlet and Cailletaud [43] changed the recovery term of the AF hardening rule and proposed their rule in the form of:

$$d\alpha = \frac{2}{3} B d\epsilon^p - \gamma (\alpha \cdot n) n dp$$

$$n = \frac{\partial f / \partial \sigma}{|\partial f / \partial \sigma|} = \frac{\bar{s}}{R_0} \tag{7}$$

$$dp = \sqrt{\frac{2}{3} d\epsilon^p d\epsilon^p} = \sqrt{\frac{2}{3}} d\lambda$$

where, n is in the direction of the gradient of the yield surface. Since an associated flow rule is assumed for the model, $d\epsilon^p$ and n will attain the same direction and therefore, the backstress will evolve in the direction of \bar{s} .

3. 3. The Nonlinear Hardening Rule Presented By Bari and Hassan

Bari and Hassan [36] used a linear combination of the Armstrong-Frederick and the Burlet-Cailletaud recovery terms to propose the following evolution law:

$$d\alpha = \sum d\alpha_i$$

$$d\alpha_i = \frac{2}{3} B_i d\epsilon^p - \gamma_i [\delta_i \alpha_i + (1 - \delta_i) (\alpha_i \cdot n) n] dp \tag{9}$$

where, δ is a proportionality coefficient designating the influence of each recovery term.

4. STABILIZATION OF HARDENING RULES

The term stabilized is used hereafter to define the state which the hardening rule reaches, and which afterwards, the backstress tends to translate on a fixed direction. The stabilizing characteristics of hardening rules will play an important role in the calibration process which will be discussed later on.

For a von Mises plasticity model with hardening, a proportional loading path is assumed in the following form:

$$(\sigma_1, \sigma_2, \sigma_3) = (A_1 t + C_1, A_2 t + C_2, A_3 t + C_3) \tag{10}$$

Translating this loading path into deviatoric components, it can be rewritten in the form:

$$(s_1, s_2, s_3) = (D_1 t + E_1, D_2 t + E_2, D_3 t + E_3)$$

$$D_i = \left[A_i - \frac{1}{3} \sum_{k=1}^3 A_k \right] \tag{11}$$

$$E_i = \left[C_i - \frac{1}{3} \sum_{k=1}^3 C_k \right]$$

It can be proven that for a single component hardening rule of Armstrong-Frederick or Burlet-Cailletaud, with any given state of stress and backstress, if deviatoric stress components evolve according to

Equation (11), the backstress will tend to evolve in the same direction. Therefore, the following will be valid:

$$\lim_{t \rightarrow \infty} da = ds = (D_1, D_2, D_3) dt \tag{12}$$

Proof to this relation is given in the appendix. The significance of the proof is that it is independent of the initial state of stress and backstress. Therefore, it will be effectively valid during load reversals, as long as the stress variation remains on the same path.

In order to gain more insight into the stabilization characteristic of single component hardening rules, the loading history of Figure 1a with the loading values of test-2 is considered. It should be noted that while the loading in one direction is a constant stress, it is a varying strain in the other direction. Applying this strain would imply the presence of an induced stress which varies through time.

The response of different hardening rules is presented in the deviatoric plane (Figure 2). This figure illustrates the trace of the backstress during the first few cycles of this loading history. As can be seen in this figure, both Armstrong-Frederick and Burlet-Cailletaud hardening rules become stabilized during these cycles. However, it takes more cycles for the BC model to stabilize than the AF model. It should be noted that the following hardening parameters are used for both models:

$$B = 62,750 \text{ MPa} \quad , \gamma = 552.5$$

In addition, given in this figure, it is the response of a single component hardening rule in the form of Equation (9), where the same hardening parameters are used and the proportionality coefficient is set to $\delta = 0.5$. It can be seen that this hardening rule does not completely stabilize. However, its variation is bound between the other two hardening rules. In order to take advantage of these observations, the linear equation of the stress and stabilized backstress paths are required. For this purpose, a rectangular coordinate system (ξ, ζ) is attached to the origin of the deviatoric plane coordinate system (s'_1, s'_2, s'_3) of Figure 2 and the translating relations are acquired. This new coordinate system is illustrated in Figure 3.

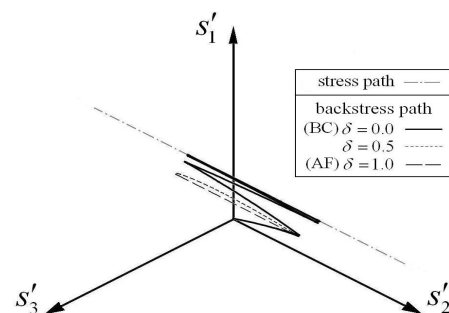


Figure 2. Stabilization of hardening rules and traces of the backstress.

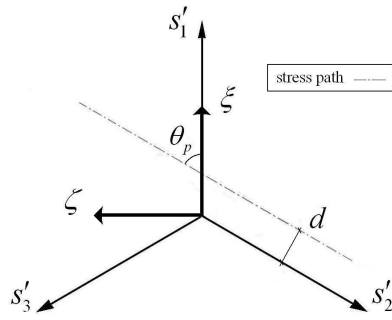


Figure 3. The (ξ, ζ) coordinate system in the deviatoric plane

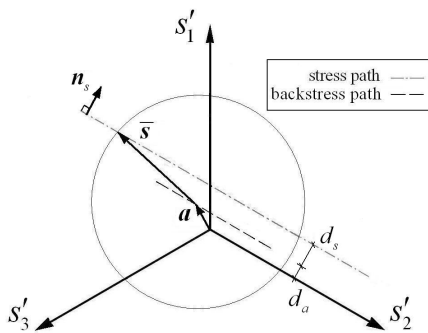


Figure 4. Stress and backstress states and stabilization parameters.

Knowing that the (s'_1, s'_2, s'_3) axes are actually the projections of the (s_1, s_2, s_3) axes onto the deviatoric plane, one can write $s'_i = \sqrt{2/3}s_i$. Furthermore, by calculating the (ξ, ζ) components of (s'_1, s'_2, s'_3) and using Equation (11), the following relations are obtained:

$$\begin{cases} \xi = \sqrt{\frac{3}{2}}s_1 = \sqrt{\frac{3}{2}}(D_1t + E_1) \\ \zeta = \frac{\sqrt{2}}{2}(s_3 - s_2) = \frac{\sqrt{2}}{2}[(D_2 + D_3)t + (E_2 + E_3)] \end{cases} \quad (13)$$

At this point, the distance between the origin and the stress path can be calculated (Figure 3). This distance will be denoted by d in the succeeding text. Referring to the general hardening rule of Equation (9), one can say that the direction which the backstress translates is a combination of the vectors \bar{s} (or $d\epsilon^p$) and \mathbf{a} . Therefore, the following relation will be valid:

$$\frac{d\mathbf{a}}{d\lambda} = [G_1 - G'_1(\bar{s} \cdot \mathbf{a})]\bar{s} - G_2\mathbf{a} \quad (14)$$

where,

$$G_1 = \frac{2}{3} \frac{B}{R_0}, \quad G'_1 = \sqrt{\frac{2}{3}} \frac{(1-\delta)\gamma}{R_0^2}, \quad G_2 = \sqrt{\frac{2}{3}}(\delta)\gamma \quad (15)$$

The vectors \bar{s} and \mathbf{a} are depicted in Figure 4 for an arbitrary point. Furthermore, demonstrated in this figure

is the stress path, the backstress path and the vector \mathbf{n}_s which is a unit vector, normal to the stress path.

Equation (12) has only been proven for a hardening rule which is in the form of Equations (6) or (7) and is not valid for the combination of these hardening rules defined by Equation (9). However, the numerical results for a symmetrical strain-controlled cyclic loading imply that for the hardening rule of Equation (9), two assumptions can be made:

– **Assumption 1.** The trace of the backstress is a straight line parallel to the stress path.

– **Assumption 2.** The effective value of $(\bar{s} \cdot \mathbf{a})$ is equal

$$\text{to } 0.5[d_a d_s + \sqrt{2/3}(B/\gamma)R_0].$$

where, d_a is the distance between the stabilized backstress path and the origin, and d_s is the distance between the stress path and the backstress path. The reason to the first assumption is evident from Figure 2. However, the second assumption is a conclusion to the first one and its rationale is provided in the appendix. While these assumptions are introduced to simplify future mathematical manipulations, numerical examples have shown that they are reasonable and yield good results.

Using the abovementioned assumptions and the fact that \mathbf{n}_s is normal to the stress path, the following relations will be valid after stabilization:

$$\begin{aligned} \mathbf{n}_s \cdot d\mathbf{s} &= 0 \\ \rightarrow \mathbf{n}_s \cdot d\mathbf{a} &= 0 \\ \rightarrow \mathbf{n}_s \cdot [G_1\bar{s} - G_2\mathbf{a} - 0.5G'_1(d_a d_s + \sqrt{2/3}(B/\gamma)R_0)\bar{s}] &= 0 \\ \rightarrow G_1 d_s - G_2(d - d_s) - 0.5G'_1 d_s (d - d_s) &= 0 \end{aligned} \quad (16)$$

where, $d = d_a + d_s = \mathbf{n}_s \cdot \mathbf{s}$ is the distance between the stress path and the origin, $d_a = \mathbf{n}_s \cdot \mathbf{a}$ is the distance between the stabilized path of the backstress and the origin, and $d_s = \mathbf{n}_s \cdot \bar{s}$ is the distance between the stress path and the stabilized backstress path (Figure 4).

Another property noticed from these results is that after the backstress stabilizes, the direction of the vector \bar{s} remains the same. This will be true until the loading is reversed, which from that point, the direction of \bar{s} will be fixed in another direction (the direction of \bar{s} during reversed loadings is symmetrical with respect to \mathbf{n}_s). This is an important fact, since the plastic strain increment ($d\epsilon^p$) is in the direction of \bar{s} and therefore, its direction will also be fixed. In order to find the direction of \bar{s} after stabilization, the vector \mathbf{n}_s is used.

Knowing that $|\bar{s}| = \sqrt{2J_2} = R_0$, the following equation can be used:

$$\begin{aligned} \mathbf{n}_s \cdot \bar{\mathbf{s}} &= |\mathbf{n}_s| |\bar{\mathbf{s}}| \cos \theta_s = d_s \\ \rightarrow \cos \theta_s &= \frac{d_s}{R_0} = \frac{d-d_a}{R_0} \end{aligned} \quad (17)$$

where, θ_s would be the angle between $\bar{\mathbf{s}}$ and \mathbf{n}_s . The above equation will give two opposite values for θ_s , which indicate the symmetry of $\bar{\mathbf{s}}$ with respect to \mathbf{n}_s , during reversed loadings. After calculating the angle θ_p , between the stress path and the ξ axis (or actually the s'_1 axis) using Equation (13), the following relations can be obtained for the angle of $\bar{\mathbf{s}}$ with each of the deviatoric plane axes (s'_1, s'_2, s'_3):

$$\begin{aligned} \theta_p &= \tan^{-1} \frac{\sqrt{3}D_1}{D_2 + D_3} \\ \begin{cases} \theta_1 = (\frac{\pi}{2} - \theta_s) - \theta_p \\ \theta_2 = (\theta_s - \frac{\pi}{4}) - \theta_p \\ \theta_3 = (\theta_s - \frac{\pi}{2}) - \theta_p \end{cases} \end{aligned} \quad (18)$$

By introducing a single component of Equation (9) into Equation (3) and taking advantage of Equation (4), the following can be obtained for $d\lambda$:

$$d\lambda = \frac{\bar{\mathbf{s}} \cdot d\mathbf{s}}{\frac{2}{3}BR_0 - \gamma(\bar{\mathbf{s}} \cdot \boldsymbol{\alpha})\sqrt{\frac{2}{3}}} \quad (19)$$

Knowing that \mathbf{n}_s is normal to $d\mathbf{s}$, the angle between $\bar{\mathbf{s}}$ and $d\mathbf{s}$ is reckoned to be equal to $\pi/2 - \theta_s$, therefore:

$$d\lambda = \frac{|\bar{\mathbf{s}}| |d\mathbf{s}| \cos\left(\frac{\pi}{2} - \theta_s\right)}{\frac{2}{3}BR_0 - \gamma(\bar{\mathbf{s}} \cdot \boldsymbol{\alpha})\sqrt{\frac{2}{3}}} \quad (20)$$

Finally, using Equation (11), the above equation can be rewritten as:

$$d\lambda = \frac{\sqrt{D_1^2 + D_2^2 + D_3^2} \sin \theta_s}{\frac{2}{3}B - \gamma \frac{(\bar{\mathbf{s}} \cdot \boldsymbol{\alpha})}{R_0} \sqrt{\frac{2}{3}}} dt \quad (21)$$

For a strain controlled cyclic loading, this equation cannot be directly used, since it's based on knowing the variations of stress rather than strain. However, due to the fact that the loading is cyclic and symmetrical, Equation (21) has a significant outcome. While the second assumption made before states that the effective value of $(\bar{\mathbf{s}} \cdot \boldsymbol{\alpha})$ is equal to $0.5[d_a d_s + \sqrt{2/3}(B/\gamma)R_0]$, referring to the proof provided for it in the appendix, it can be shown that the average value of $(\bar{\mathbf{s}} \cdot \boldsymbol{\alpha})$ during a complete cycle of loading is equal to $d_a d_s$. Therefore, after integration of Equation (21), the following can be written:

$$\Delta\lambda = \int_{\Delta t} d\lambda \approx \frac{\sqrt{D_1^2 + D_2^2 + D_3^2} \sin \theta_s \Delta t}{\frac{2}{3}B - \gamma \frac{d_a d_s}{R_0} \sqrt{\frac{2}{3}}} \quad (22)$$

For commonly used values of B and γ and reasonable loading histories, the second term in the denominator of the above equation will be small compared to the first term. Therefore, Equation (22) can be approximated with:

$$\Delta\lambda \approx \frac{3\sqrt{D_1^2 + D_2^2 + D_3^2} \sin \theta_s \Delta t}{2B} \quad (23)$$

This estimation has proven to be quite accurate. The equation indicates that $\Delta\lambda$ has a linear relation with $\sin \theta_s$, and that it will also attain the same value for the positive and negative phases of a cycle.

5. CALIBRATION OF δ FOR A SINGLE COMPONENT HARDENING RULE

The process of calibrating the constant δ will be discussed in this section. This method will be based on the loading history illustrated in Figure 1a, where a constant stress is present in one direction (σ_1) and a symmetrical cyclic axial strain (ε_{2c}) is applied in the other direction. This loading history is the simplest biaxial loading history that can be carried out in experimental studies. Therefore, it will be a good case for the calibration of the hardening parameters. Experimental results regarding this loading case conducted on various materials can be found in the literature. The well-known experimental data reported in [7] and [13] on the biaxial behavior of CS1026 will be used in the present work. It should also be mentioned that in the proceeding text, it is assumed that the values of B and γ have already been calibrated for uniaxial ratcheting.

Since the accumulated plastic strain in the direction of the constant stress is reported for each cycle, the first principle component of $\boldsymbol{\varepsilon}^p$ will be needed. Referring to Equation (4), the following equation can be written:

$$d\varepsilon_1^p = d\varepsilon_1^p = d\lambda \frac{\bar{s}_1}{R_0} = d\lambda \cos \theta_1 \quad (24)$$

where, θ_1 is the angle between $\bar{\mathbf{s}}$ and the s'_1 axis. Based on Equation (18), the above equation will take the following form:

$$\begin{aligned} d\varepsilon_1^p &= d\varepsilon_1^p = d\lambda \cos\left[\left(\frac{\pi}{2} - \theta_s\right) - \theta_p\right] \\ &= d\lambda \sin(\theta_s + \theta_p) \end{aligned} \quad (25)$$

After introducing Equation (23) into the above equation and then integrating for the positive and negative phases of loading, the following equation will be obtained:

$$\begin{cases} (\Delta \varepsilon_1^p)_{pos} \\ = \frac{3\sqrt{D_1^2 + D_2^2 + D_3^2}}{2B} \sin(\theta_s) \sin(\theta_s + \theta_p) \Delta t \\ (\Delta \varepsilon_1^p)_{neg} \\ = \frac{3\sqrt{D_1^2 + D_2^2 + D_3^2}}{2B} \sin(-\theta_s) \sin(-\theta_s + \theta_p) \Delta t \end{cases} \quad (26)$$

By adding the plastic strain increment of the two phases and performing some mathematical manipulation, the total plastic strain increment of one cycle is obtained as follows:

$$\Delta \varepsilon_1^p = \frac{3\sqrt{D_1^2 + D_2^2 + D_3^2}}{2B} \sin(\theta_p) \sin(2\theta_s) \Delta t \quad (27)$$

This equation cannot be directly used for a strain-controlled loading. However, it implies that the plastic strain increment has a linear relation with $\sin(\theta_p) \sin(2\theta_s)$, which will be used for the calibration process. Equations (15) and (16) indicate that for a Burlet-Cailletaud hardening rule where $\delta = 0$, the value of d_s will be equal to zero. Introducing this into Equation (17) will lead to $\theta_s = \pm\pi/2$. Therefore, by utilizing Equation (27), it can be shown that for $\delta = 0$, the total plastic strain increment during one cycle is $(\Delta \varepsilon_1^p)_{BC} = 0$. For the Armstrong-Frederick hardening rule ($\delta = 1$), by knowing the values of B and γ , the value of $(\Delta \varepsilon_1^p)_{AF}$ can be numerically determined. Considering these values for $(\Delta \varepsilon_1^p)_{BC}$ and $(\Delta \varepsilon_1^p)_{AF}$, and making use of Equations (17) and (27), the following relation can be written for an arbitrary value of $0 < \delta < 1$:

$$\left[\frac{\Delta \varepsilon_1^p}{\sin(2\theta_s)} \right]_{AF} = \left[\frac{\Delta \varepsilon_1^p}{\sin(2\theta_s)} \right]_{\delta} \quad (28)$$

In this equation, $(\theta_s)_{AF}$ is evaluated using Equations (16) and (17), $(\Delta \varepsilon_1^p)_{AF}$ is numerically determined from a single cycle plastic analysis and $(\Delta \varepsilon_1^p)_{\delta}$ is extracted from experimental data. Knowing these values, Equation (28) can be used to obtain $(\theta_s)_{\delta}$. Introducing this value into Equation (17), the value of $(d_s)_{\delta}$ can be determined. Finally, using Equations (15) and (16), δ will be attainable. Based on this process, a step by step approach to the calibration procedure is presented below. As an example for this section, a single component hardening rule in the form of Equation (9) will be calibrated using the biaxial response of CS1026 reported in [7]. The mathematical process will be according to the abovementioned algorithm. Six different sets of $(\sigma_{1m}, \varepsilon_{2c})$ for the loading history of Figure 1a which are covered in the experiments are given in Table 1. The calibrating process will be carried out for Test-2. It is also assumed that the values of B and γ have already been calibrated for uniaxial

TABLE 3. Step by step procedure for the calibration process.

1. Obtain B and γ for a single-component AF hardening rule.
2. Solve Equation (16) with $\delta = 1$ for $(d_s)_{AF}$.
3. Calculate $(\theta_s)_{AF}$ using Equation (17)
4. Calculate $(\Delta \varepsilon_1^p)_{AF}$ numerically.
5. Evaluate $(\Delta \varepsilon_1^p)_{\delta}$ from experimental data.
6. Calculate $(\theta_s)_{\delta}$ using Equation (28).
7. Calculate $(d_s)_{\delta}$ using Equation (17).
8. Solve Equations (15) and (16) for δ .

ratcheting simulation, using the method proposed in [42] for an Armstrong-Frederick model. Since this has already been done in the mentioned article for CS1026, the process will not be repeated here and the result, which is the following values, will be used.

$$E = 181,300 \text{ MPa}, \nu = 0.302, \sigma_y = 186.2 \text{ MPa}$$

$$B = 62,750 \text{ MPa}, \gamma = 552.5$$

For the loading history of Test-2 the values of D_i and E_i defined in Equation (11) are determined as below:

$$D_1 = -0.333 \text{ (MPa/s)}, E_1 = +44.333 \text{ (MPa)}$$

$$D_2 = +0.667, E_2 = -22.167$$

$$D_3 = -0.333, E_3 = -22.167$$

Using these values, the distance of the deviatoric stress path from the origin is calculated to be $d = 47.0 \text{ MPa}$. For a single component AF hardening rule with the abovementioned values for the hardening parameters, the values of $(\Delta \varepsilon_1^p)_{AF}$, $(d_s)_{AF}$ and $(\theta_s)_{AF}$ are determined after stabilization, leading to:

$$(\Delta \varepsilon_1^p)_{AF} = 0.229 \text{ (\%)} \\ (d_s)_{AF} = 29.4 \text{ (MPa)} \\ (\theta_s)_{AF} = 78.86^\circ = 1.376 \text{ (rad)}$$

In addition, from the results given by Hassan et al. (1992), the overall value of the plastic strain increment during one cycle of this loading history is evaluated to be equal to $\Delta \varepsilon_1^p = 0.055 \text{ (\%)}$. This will be the value of plastic strain increment that δ should be determined according to.

The abovementioned results obtained from the AF hardening rule and the value of $(\Delta \varepsilon_1^p)_{\delta} = 0.06 \text{ (\%)}$ are introduced into Equation (28) and the equation is solved for $(\theta_s)_{\delta}$. The result is introduced into Equation (17) to obtain $(d_s)_{\delta}$. Finally, by introducing this value of $(d_s)_{\delta}$ into Equation (16) and using Equation (15), the resulting equation

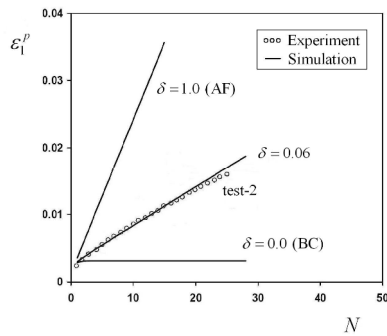
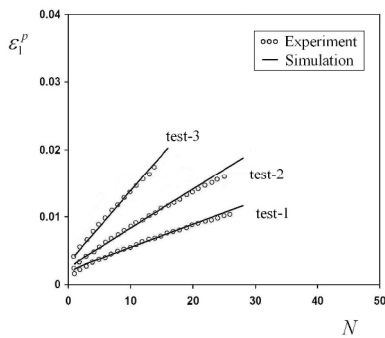
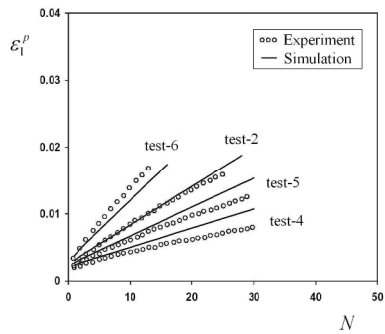


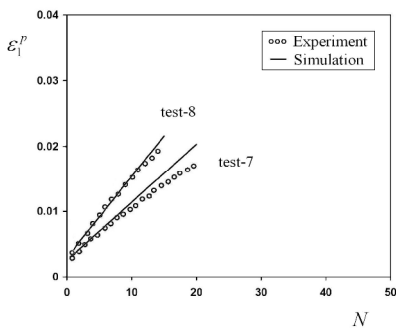
Figure 5. Ratcheting predictions using different values of δ



(a)



(b)



(c)

Figure 6. Comparison of ratcheting predictions using the single-component hardening model with experimental data from [7] and [13]. (a,b) axial strain cycle with constant internal pressure. (c) bow-tie cycle.

can be solved to determine δ . The results of this procedure are presented below:

$$(\theta_s)_\delta = 87.18^\circ = 1.522 \text{ (rad)}$$

$$(d_s)_\delta = 7.47 \text{ (MPa)}$$

$$\delta = 0.060$$

Figure 5 illustrates the results obtained for a single component hardening rule using three values of δ . The analysis is based on the loading history of Figure 1a with the loading values of test-2 depicted in Table 1. This figure shows the effect of δ on the ratcheting response of the model.

Figures 6a and 6b illustrate the response of a single component hardening rule with $\delta = 0.06$, compared to the experimental data resulting from the axial strain cycle with constant internal pressure loading history given in Figure 1a. Figure 6c compares the analytical results of the bow-tie loading history (Figure 1b) to experimental data.

6. CALIBRATION OF δ FOR A MULTI-COMPONENT HARDENING RULE

The calibration procedure developed in [42] is based on a sequential method of adding backstress components to the hardening rule and determining the hardening parameters in such a way that the new model improves the previous one. Therefore, constructing a multi-component hardening rule (N3-L1) based on their procedure will not affect the main characteristics of the previous single component model (AF), but will only eliminate its deficiencies (mainly in the uniaxial response). According to this, it would be reasonable to apply the same value of δ obtained in the previous section, to the multi-component model as well. Since the parameters of a four-component hardening rule have already been determined for CS1026 in [42], the process will not be repeated here and the following values, adopted from their results, will be used:

$$E = 181,300 \text{ MPa}, \nu = 0.302, \sigma_y = 186.2 \text{ MPa}$$

$$B_1 = 56,330 \text{ MPa}, \gamma_1 = 680.9$$

$$B_2 = 8710 \text{ MPa}, \gamma_2 = 841.7$$

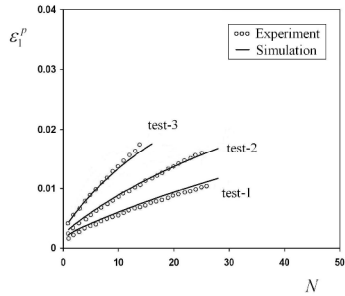
$$B_3 = 1100 \text{ MPa}, \gamma_3 = 35.5$$

$$B_4 = 1100 \text{ MPa}$$

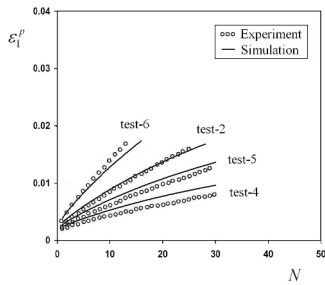
$$\text{with } \delta = 0.06$$

Figures 7a and b illustrate the response of the multi-component hardening rule with $\delta = 0.06$, compared to the experimental data resulting from the axial strain cycle with constant internal pressure loading history given in Figure 1a. Figures 7c and d show the predictions obtained in [36] for comparison. They also used a four-component hardening rule to simulate the same experiments. Figure 8a compares the analytical results of the bow-tie loading history (Figure 1b) to

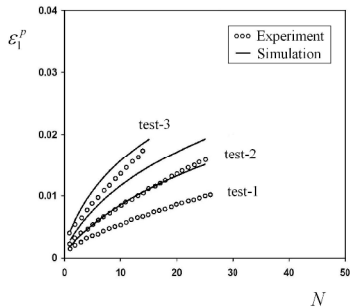
experimental data using the hardening parameters obtained in the present work. Figure 8b shows the predictions obtained by Bari and Hassan (2002) for the same experiment, using a four-component hardening rule.



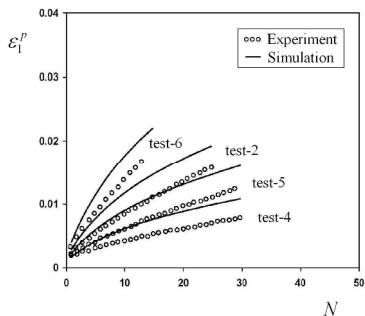
(a)



(b)

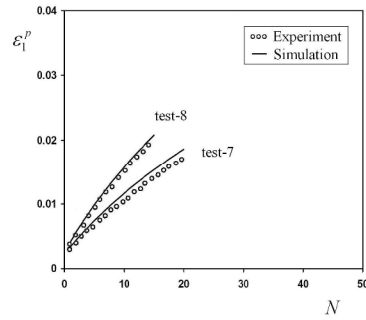


(c)

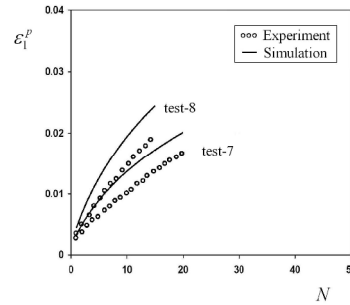


(d)

Figure 7. Comparison of ratcheting predictions using a four-component hardening model with experimental data from [7]. (a, b) Simulation using the hardening parameters obtained in this paper. (c, d) Simulation using the hardening parameters obtained in [36].



(a)



(b)

Figure 8. Comparison of ratcheting predictions using a four-component hardening model with experimental data from [13]. (a, b) Simulation using the hardening parameters obtained in this paper.

7. CONCLUSION

A systematic approach is developed to determine the multi-axial hardening parameter δ used in multi-axial ratcheting simulation. This is achieved by taking advantage of key characteristics of kinematic hardening models during cyclic loading. Mathematical proof is provided for these characteristics. While simplifying assumptions are made to lay out the mathematical groundwork of the method, numerical analyses have shown that the assumptions do not affect the efficiency of the solution.

The present work is completely consistent with the calibration technique previously presented by the authors [42] for uniaxial ratcheting simulation. Put together, these methods provide a clear-cut and effective algorithm to calibrate hardening parameters for multi-axial ratcheting. The significance of this algorithm is that unlike current parameter determination techniques, it does not involve trial and error to produce acceptable results. Numerical examples have been carried out using the experimental data of [7] and [13]. The results are compared to the ones obtained by Bari and Hassan [36] which also used a four-component hardening rule to simulate the same experiments. These examples demonstrate the effectiveness of the method. In addition, the results indicate that multi-component

hardening rules can be much more efficient in multi-axial ratcheting prediction than what has been shown before, if they are calibrated using this technique.

8. ACKNOWLEDGEMENT

The authors greatly acknowledge the grant provided by the Ferdowsi University of Mashhad for the financial support of this work.

9. REFERENCES

- Moyar, G. J. and Sinclair, G.M., "Cyclic strain accumulation under complex multiaxial loading", In: Proceedings of the Joint International Conference on Creep, Institution of Mechanical Engineers, London, (1963), 2-47.
- Benham, P. P., "Some observations on the cyclic strain-induced creep in mild steel at room temperature", *International Journal of Mechanical Sciences*, Vol. 7, (1965), 81-86.
- Freudenthal, A. M. and Ronay, M., "Second order effects in dissipative media", *Proceedings of the Royal Society of London. Series A. Mathematical and Physical Sciences*, Vol. 292, (1966), 14-50.
- Ruiz, C., "High-strain fatigue of stainless-steel cylinders: experimental results and their application to pressure-vessel design", *Journal of Strain Analysis*, Vol. 2, (1967), 290.
- Yoshida, F., Tajima, N., Ikegami, K. and Shiratori, E., "Plastic theory of the mechanical ratcheting", *Bulletin of the JSME*, Vol. 21, (1978), 389-397.
- Benallal, A. and Le Gallo, P., "Marquis D., An experimental investigation of cyclic hardening of 316 stainless steel and of 2024 aluminum alloy under multiaxial loading", *Nuclear Engineering and Design*, Vol. 114, (1989), 345-353.
- Hassan, T., Corona, E. and Kyriakides, S., "Ratcheting in cyclic plasticity, part II: Multiaxial behavior", *International Journal of Plasticity*, Vol. 8, (1992), 117-146.
- Hassan, T. and Kyriakides, S., "Ratcheting in cyclic plasticity, part I: Uniaxial behavior", *International Journal of Plasticity*, Vol. 8, (1992), 91-116.
- Hassan, T. and Kyriakides, S., "Ratcheting of cyclically hardening and softening materials, part I: Uniaxial behavior", *International Journal of Plasticity*, Vol. 10, (1994), 149-184.
- Hassan, T. and Kyriakides, S., "Ratcheting of cyclically hardening and softening materials, part II: Multiaxial behavior", *International Journal of Plasticity*, Vol. 10, (1994), 185-212.
- Yoshida, F., "Ratcheting behavior of 304 stainless steel at 650°C under multiaxial strain-controlled and uniaxially/multiaxially stress-controlled conditions", *European Journal of Mechanics-A/Solids*, Vol. 14, (1995), 97-117.
- Delobelle, P., Robinet, P. and Bocher, L., "Experimental study and phenomenological modelization of ratcheting under uniaxial and biaxial loading on an austenitic stainless steel", *International Journal of Plasticity*, Vol. 11, (1995), 295-330.
- Corona, E., Hassan, T. and Kyriakides, S., "On the performance of kinematic hardening rules in predicting a class of biaxial ratcheting histories", *International Journal of Plasticity*, Vol. 12, (1996), 117-145.
- Portier, L., Calloch, S., Marquis, D. and Geyer, P., "Ratcheting under tension-torsion loadings: Experiments and modeling", *International Journal of Plasticity*, Vol. 16, (2000), 303-335.
- Bocher, L., Delobelle, P., Robinet, P. and Feaugas, X., "Mechanical and microstructural investigations of an austenitic stainless steel under non-proportional loadings in tension-torsion-internal and external pressure", *International Journal of Plasticity*, Vol. 17, (2001), 1491-1530.
- Aubin, V., Quaegebeur, P. and Degallaix S., "Cyclic plasticity of a duplex stainless steel under non-proportional loading", *Material Science and Engineering A346*, (2003), 208-215.
- Kang, G. Z., Gao, Q. and Yang, X. J., "Uniaxial and nonproportional multiaxial ratcheting of SS304 stainless steel at room temperature: Experiments and simulations", *International Journal of Non-linear Mechanics*, Vol. 39, (2004), 843-857.
- Hassan, T., Taleb, L. and Krishna, S., "Influence of non-proportional loading on ratcheting responses and simulations by two recent cyclic plasticity models", *International Journal of Plasticity*, Vol. 24, (2008), 1863-1889.
- Prager, W., "A new method of analyzing stresses and strains in work hardening plastic solids", *Journal of Applied Mechanics*, Vol. 23, (1956), 493-496.
- Besseling, J. F., "A theory of elastic, plastic, and creep deformations of an initially isotropic material", *ASME Journal of Applied Mechanics*, Vol. 25, (1958), 529-536.
- Mroz, Z., "On the description of anisotropic work hardening", *Journal of Mechanics and Physics of Solids*, Vol. 15, (1967), 163-175.
- Dafalias, Y. F. and Popov, E. P., "A model of nonlinearly hardening materials for complex loading", In: *Proceedings of the 7th US National Congress of Theoretical and Applied Mechanics*, Boulder, Colorado, (1974), 149.
- Dafalias, Y. F. and Popov, E. P., "A model of nonlinearly hardening materials for complex loading", *Acta Mechanica*, Vol. 21, (1975), 173-192.
- Dafalias, Y. F. and Popov, E. P., "Plastic internal variables formalism of cyclic plasticity", *ASME Journal of Applied Mechanics*, Vol. 43, (1976), 645-650.
- Krieg, R. D., "A practical two-surface plasticity theory", *ASME Journal of Applied Mechanics*, Vol. 42, (1975), 641-646.
- Dafalias, Y. F., "Bounding surface plasticity. Part I: Mathematical foundation and hypoplasticity", *ASCE Journal of Engineering Mechanics*, Vol. 112, (1986), 966-987.
- Armstrong, P. J. and Frederick, C. O., "A Mathematical representation of the multiaxial bausinger effect", Cegb Report No. Rd/B/N 731, (1966).
- Chaboche, J. L., Dang-Van, K. and Cordier, G., "Modelization of strain memory effect on the cyclic hardening of 316 stainless steel", In: Transactions of the 5th International Conference on Structural Mechanics in Reactor Technology, Berlin, no. Div L in 11/3, (1979).
- Chaboche, J. L., "Time-independent constitutive theories for cyclic plasticity", *International Journal of Plasticity*, Vol. 2, (1986), 149-188.
- Chaboche, J. L., "On some modifications of kinematic hardening to improve the description of ratcheting effects", *International Journal of Plasticity*, Vol. 7, (1991), 661-678.
- Ohno, N. and Wang, J. D., "Kinematic hardening rules with critical state of dynamic recovery, part I: Formulations and basic features for ratcheting behavior", *International Journal of Plasticity*, Vol. 9, (1993), 375-390.
- Medowell, D. L., "Stress state dependence of cyclic ratcheting behavior of two rail steels", *International Journal of Plasticity*, Vol. 11, (1995), 397-421.
- Jiang, Y. and Sehitoglu, H., "Modeling of cyclic ratcheting plasticity, part I: Development of constitutive relations", *ASME Journal of Applied Mechanics*, Vol. 63, (1996), 720-725.

34. Voyiadjis, G. Z. and Basuroychowdhury, I. N., "A plasticity model for multiaxial cyclic loading and ratcheting", *Acta Mechanica*, Vol. 126, (1998), 19-35.
35. Abdelkarim, M. and Ohno, N., "Kinematic hardening model Suitable for ratcheting with steady-State", *International Journal of Plasticity*, Vol. 16, (2000), 225-240.
36. Bari, S. and Hassan, T., "An advancement in cyclic plasticity modeling for multiaxial ratcheting simulation", *International Journal of Plasticity*, Vol. 18, (2002), 873-894.
37. Chen, X. and Jiao, R., "Modified kinematic hardening rule for multiaxial ratcheting prediction", *International Journal of Plasticity*, Vol. 20, (2004), 871-898.
38. Chen, X, Jiao, R. and Kim, K. S., "On the ohno-wang kinematic hardening rules for multiaxial ratcheting modeling of medium carbon steel", *International Journal of Plasticity*, Vol. 21, (2005), 161-184.
39. Chaboche, J. L., "A review of some plasticity and viscoplasticity constitutive theories", *International Journal of Plasticity*, Vol. 24, (2008), 1642-1693.
40. Bari, S. and Hassan, T., "Anatomy of coupled constitutive models for ratcheting simulation", *International Journal of Plasticity*, Vol. 16, (2000), 381-409.
41. Koo, G. H. and Lee, J. H., "Investigation of ratcheting characteristics of modified 9Cr-1Mo steel by using the Chaboche constitutive model", *International Journal of Pressure Vessels and Piping*, Vol. 84, (2007), 284-292.
42. Rezaiee-Pajand, M. and Sinaie, S., "On the calibration of the Chaboche hardening model and a modified hardening rule for uniaxial ratcheting prediction", *International Journal of Solids and Structures*, Vol. 46, (2009), 3009-3017.
43. Burlet, H. and Cailletaud, G., "Numerical techniques for cyclic plasticity at variable temperature", *Engineering Computations*, Vol. 3, (1986), 143-153.

APPENDIX A

A. 1. Proof to Equation (12)

In the following sections, mathematical proof is provided for Equation (12). This is achieved independently for the Burlet-Cailletaud model (Equation (7)) and the Armstrong-Frederick model (Equation (6)).

A. 1. 1. Stabilization of the Burlet-Cailletaud Hardening Rule Using the general relation given in Equation (3), the following can be obtained:

$$(\bar{s} \cdot ds - \bar{s} \cdot da)\bar{s} = (\bar{s} \cdot ds)\bar{s} - (\bar{s} \cdot da)\bar{s} = 0 \quad (\text{A.1})$$

For the Burlet-Cailletaud hardening rule (or even Prager's hardening rule) where the backstress evolves in the direction of the plastic strain increment, the vectors

of da and \bar{s} will be in the same direction. Therefore, $(\bar{s} \cdot da)\bar{s} = (\bar{s} \cdot \bar{s})da$. Hence, Equation (A.1) can be rewritten as:

$$\begin{aligned} (\bar{s} \cdot ds)\bar{s} - (\bar{s} \cdot \bar{s})da &= 0 \\ \rightarrow da &= \frac{(\bar{s} \cdot ds)\bar{s}}{|\bar{s}|^2} \end{aligned} \quad (\text{A.2})$$

which gives the direction of the backstress evolution. Considering Figure 4, the following can be written for the angle between the vectors of ds and \bar{s} :

$$f(\bar{s}) = \cos \theta = \frac{\bar{s} \cdot ds}{|\bar{s}| |ds|} \quad (\text{A.3})$$

where, $||$ denotes the magnitude of a vector. Since the direction of the deviatoric stress increments is assumed to be constant (Equation (11)), this angle will only be a function of \bar{s} . Reminding that the size of yield surface is assumed to be constant, \bar{s} will not change in magnitude but only in direction. A differential change in \bar{s} will result in:

$$\begin{aligned} f(\bar{s} + d\bar{s}) &= f(\bar{s}) + \frac{\partial f(\bar{s})}{\partial \bar{s}} d\bar{s} \\ &= f(\bar{s}) + \frac{d\bar{s} \cdot ds}{|\bar{s}| |ds|} = f(\bar{s}) + \frac{(ds - da) \cdot ds}{|\bar{s}| |ds|} \end{aligned} \quad (\text{A.4})$$

By introducing the relation given for da in Equation (A.2) into the above equation, the following can be obtained:

$$\begin{aligned} f(\bar{s} + d\bar{s}) &= f(\bar{s}) + \frac{(ds - da) \cdot ds}{|\bar{s}| |ds|} \\ &= f(\bar{s}) + \frac{(ds \cdot ds) - (\bar{s} \cdot ds)(\bar{s} \cdot ds)}{|\bar{s}|^3 |ds|} \\ &= f(\bar{s}) + \frac{|ds|^2 - (|\bar{s}| |ds| \cos \theta)^2}{|\bar{s}|^3 |ds|} \\ &= f(\bar{s}) + \frac{|ds|}{|\bar{s}|} (1 - \cos^2 \theta) \end{aligned} \quad (\text{A.5})$$

which indicates that the value of $f(\bar{s})$ will increase due to the changes of \bar{s} . This implies the fact that for any given state of stress and backstress, the angle between ds and \bar{s} will decrease, when the deviatoric stress state varies according to Equation (11). Since for the Burlet-Cailletaud hardening rule, da is in the direction of \bar{s} , as the angle between ds and \bar{s} approaches zero, the following can be deduced:

$$\lim_{\theta \rightarrow 0} \lim_{t \rightarrow \infty} da = ds = (D_1, D_2, D_3) dt \quad (\text{A.6})$$

A. 1. 2. Stabilization of the Armstrong-Frederick Hardening Rule The proof of Equation (12) for the Armstrong-Frederick hardening rule is quite different than for the Burlet-Cailletaud hardening rule. Using the associated flow rule assumption of Equation (4), it can

be shown that $dp = \sqrt{2/3}d\lambda$. Therefore, Equation (6) will reduce to:

$$d\mathbf{a} = \left(\frac{2}{3} B \frac{\bar{\mathbf{s}}}{R_0} - \gamma \mathbf{a} \sqrt{\frac{2}{3}} \right) d\lambda \quad (\text{A.7})$$

After introducing the above equation into Equation (3), one can write:

$$\bar{\mathbf{s}} \cdot (d\mathbf{s} - d\mathbf{a}) = \bar{\mathbf{s}} \cdot \left[d\mathbf{s} - \left(\frac{2}{3} B \frac{\bar{\mathbf{s}}}{R_0} - \gamma \mathbf{a} \sqrt{\frac{2}{3}} \right) d\lambda \right] = 0 \quad (\text{A.8})$$

With further mathematical manipulation, the above equation can be solved for $d\lambda$, leading to the following equation:

$$d\lambda = \frac{\bar{\mathbf{s}} \cdot d\mathbf{s}}{\frac{2}{3} BR_0 - \gamma(\bar{\mathbf{s}} \cdot \mathbf{a})\sqrt{\frac{2}{3}}} \quad (\text{A.9})$$

Replacing $d\lambda$ in Equation (A.7) with the above equation results in:

$$d\mathbf{a} = \frac{(\bar{\mathbf{s}} \cdot d\mathbf{s}) \left(\frac{2}{3} B \frac{\bar{\mathbf{s}}}{R_0} - \gamma \mathbf{a} \sqrt{\frac{2}{3}} \right)}{\frac{2}{3} BR_0 - \gamma(\bar{\mathbf{s}} \cdot \mathbf{a})\sqrt{\frac{2}{3}}} \quad (\text{A.10})$$

Replacing \mathbf{a} with $\mathbf{s} - \bar{\mathbf{s}}$ leads to:

$$d\mathbf{a} = \frac{(\bar{\mathbf{s}} \cdot d\mathbf{s}) \left(\frac{2}{3} B \frac{\bar{\mathbf{s}}}{R_0} - \gamma(\mathbf{s} - \bar{\mathbf{s}}) \sqrt{\frac{2}{3}} \right)}{\frac{2}{3} BR_0 - \gamma(\bar{\mathbf{s}} \cdot \mathbf{s} - R_0^2) \sqrt{\frac{2}{3}}} \quad (\text{A.11})$$

Knowing that $\bar{\mathbf{s}}$ is a tensor with a limited magnitude, if the components of the deviatoric stress tensor (\mathbf{s}) tend to increase according to Equation (11), the following can be obtained:

$$\lim_{t \rightarrow \infty} d\mathbf{a} = \lim_{t \rightarrow \infty} \frac{(\bar{\mathbf{s}} \cdot d\mathbf{s})\mathbf{s}}{(\mathbf{s} \cdot \bar{\mathbf{s}})} \quad (\text{A.12})$$

$$\lim_{t \rightarrow \infty} \mathbf{s} = (D_1 t, D_2 t, D_3 t) = (D_1, D_2, D_3)t$$

Which using $d\mathbf{s} = (D_1, D_2, D_3)dt$, the following can be written:

$$\lim_{t \rightarrow \infty} d\mathbf{a} = \lim_{t \rightarrow \infty} \frac{[\bar{\mathbf{s}} \cdot (D_1, D_2, D_3)dt]\mathbf{s}}{[\bar{\mathbf{s}} \cdot (D_1, D_2, D_3)t]} = \lim_{t \rightarrow \infty} \left(\frac{\mathbf{s}}{t} dt \right) = (D_1, D_2, D_3)dt = d\mathbf{s} \quad (\text{A.13})$$

A. 2. Rationale to the Second Assumption

Considering a single component hardening rule in the form of Equation (9), it can be understood that when $d\mathbf{a} = 0$, the vectors $\bar{\mathbf{s}}$ and \mathbf{a} will be in the same direction. The vector \mathbf{n} defined in Equation (9) will be used to denote this direction. Therefore:

$$\begin{aligned} d\mathbf{a} &= \frac{2}{3} B d\epsilon^p - \gamma \delta \mathbf{a} dp - (1 - \delta)(\mathbf{a} \cdot \mathbf{n}) \mathbf{n} dp \\ &= \left[\frac{2}{3} B \mathbf{n} - \sqrt{\frac{2}{3}} \gamma \delta |\mathbf{a}| \mathbf{n} - \sqrt{\frac{2}{3}} \gamma (1 - \delta) (|\mathbf{a}| \mathbf{n} \cdot \mathbf{n}) \mathbf{n} \right] d\lambda \\ &= \left[\frac{2}{3} B - \sqrt{\frac{2}{3}} \gamma |\mathbf{a}| \right] \mathbf{n} d\lambda \end{aligned} \quad (\text{A.14})$$

For the magnitude of $d\mathbf{a}$ to become equal to zero, the term inside the bracket must be equal to zero (during plastic flow, $d\lambda \neq 0$). This leads to the limiting magnitude of \mathbf{a} , as follows:

$$|\mathbf{a}|_{\max} = \sqrt{\frac{2}{3}} \frac{B}{\gamma} \quad (\text{A.15})$$

After the hardening rule becomes stabilized, the minimum value of $(\mathbf{a} \cdot \bar{\mathbf{s}})$ will correspond to the state indicated in Figure A1 and will be equal to $d_s d_a$. On the other hand, the maximum value of $(\mathbf{a} \cdot \bar{\mathbf{s}})$ will correspond to the other state indicated in the figure, and will be equal to $|\bar{\mathbf{s}}| |\mathbf{a}|_{\max}$. If an effective value is to be assumed between these two states, the following equation will be reasonable:

$$\begin{aligned} (\mathbf{a} \cdot \bar{\mathbf{s}})_{\text{effective}} &= \frac{1}{2} [(\mathbf{a} \cdot \bar{\mathbf{s}})_{\min} + (\mathbf{a} \cdot \bar{\mathbf{s}})_{\max}] \\ &= \frac{1}{2} \left[d_s d_a + R_0 \sqrt{\frac{2}{3}} \frac{B}{\gamma} \right] \end{aligned} \quad (\text{A.16})$$

However, it should be also mentioned that for a symmetrical cyclic loading, the average (not the effective) value of $(\mathbf{a} \cdot \bar{\mathbf{s}})$ will be equal to $d_s d_a$. This is due to the fact that the components of \mathbf{a} and $\bar{\mathbf{s}}$, which are parallel to the stress path, change directions in different phases of a cycle. This leads to positive and negative values of their product, which cancel each other during the cycle. Hence, the only components that produce an average value, will be the ones normal to the stress path, which their product is always equal to $d_s d_a$.

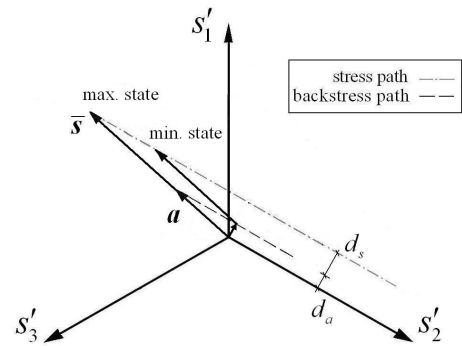


Figure A 1. Minimum and maximum states of $(\mathbf{a} \cdot \bar{\mathbf{s}})$.

Calibration of Hardening Rules for Cyclic Plasticity

M. Rezaiee-Pajand, S. Sinaie

Department of Civil Engineering, Ferdowsi University of Mashhad, Iran

PAPER INFO

چکیده

Paper history:

Received 15 July 2012

Received in revised form 04 October 2012

Accepted 18 October 2012

Keywords:

Cyclic Plasticity

Multi-axial Ratcheting

Parameter Determination

Kinematic Hardening

Calibration Methods

با هدف شبیه‌سازی چرخه‌ای چند محوری، یک شیوه‌ی گام به گام برای یافتن عامل‌های قانون‌های سخت‌شوندگی پیشنهاد می‌شود. برای رسیدن به این هدف، نخست، به ویژگی‌های قانون‌های سخت‌شوندگی پرداخته خواهد شد. سپس، این ویژگی‌ها به کار می‌روند و رابطه‌های صریحی بین تاریخچه‌ی بارگذاری و میزان کرنش مومسان به دست می‌آیند. بر خلاف روش‌های معمول، فن پیشنهادی نیازی به فرآیند آزمون و خطا ندارد. کارآمدی این راه‌کارنو با حل مثال عددی نشان داده می‌شود. نتیجه‌های عددی گویای این است که اگر عامل‌های سخت‌شوندگی به طور کارآمدی انتخاب شوند، قانون‌های سخت‌شوندگی ساده نیز توانایی زیادی برای شبیه‌سازی خزش چرخه‌ای چند محوری خواهند داشت.

doi: 10.5829/idosi.ije.2013.26.04a.04
